microPublication BIOLOGY

6/16/2026 - *Open Access*

Cryo-electron tomography reveals OmpB is required for the *Rickettsia parkeri* S-layer

Meghan C. Bacher[1], Daniel Serwas[2], Yan Han[3], Dominika Borek[4], Matthew D. Welch[1§]

[1]Department of Molecular and Cell Biology, University of California, Berkeley, Berkeley, California, United States

[2]Biohub, Redwood City, California, United States

[3]Department of Biophysics, University of Texas Southwestern Medical Center, Dallas, Texas, United States

[4]Department of Biophysics, Department of Biochemistry, University of Texas Southwestern Medical Center, Dallas, Texas, United States

[§]To whom correspondence should be addressed: welch@berkeley.edu

Abstract

Many bacteria, and most archaea, have a paracrystalline protein surface layer (S-layer) encapsulating their outer membrane or cell wall. For pathogenic *Rickettsia* species, an S-layer has been hypothesized to be comprised of the outer membrane protein OmpB. We used cryo-electron tomography (cryoET) to image the *Rickettsia parkeri* cell surface and observed a repetitive S-layer structure proximal to the outer membrane of the bacterium that is absent in an *ompB*^{STOP}::tn mutant. Our data reveal that OmpB is essential for the *Rickettsia* S-layer and suggest that we can leverage cryoET to examine rickettsial S-layer structure and function.

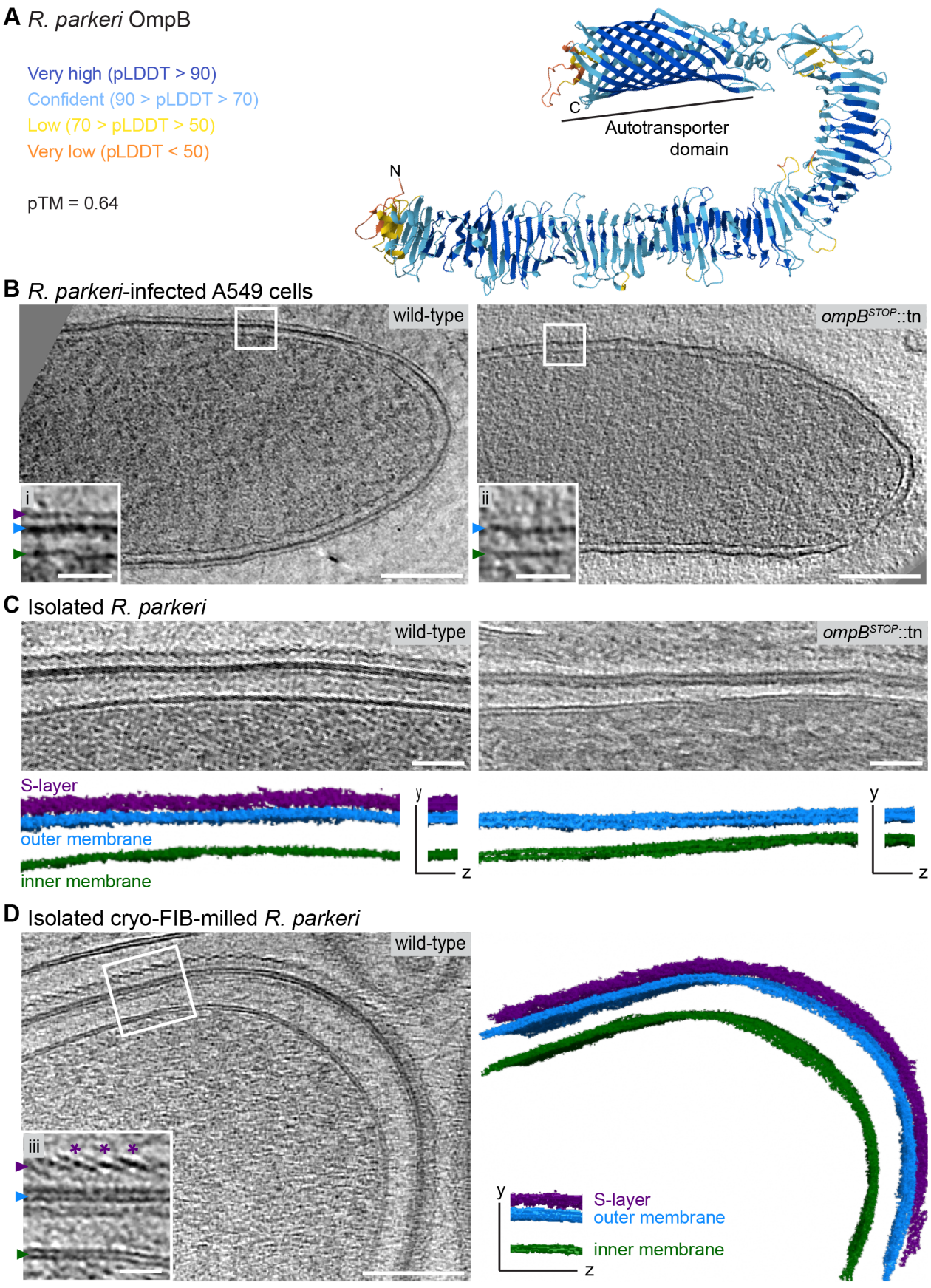

Figure 1. The surface of *R. parkeri* is encapsulated by an S-layer that is absent in *ompB*^{STOP}::tn mutant bacteria:

(A) AlphaFold 3 protein folding prediction of *R. parkeri* OmpB, color coded according to AlphaFold estimated pLDDT values (Abramson et al., 2024). (B) Tomographic slices of the surface of wild-type and *ompB*^{STOP}::tn *R. parkeri* bacteria in A549 human epithelial cells at 24 hpi. Scale bar = 200 nm. (i and ii) Insets represent magnified views of the regions of

the bacterial surface indicated in the white boxes. Arrowheads indicate the S-layer in purple, outer membrane in blue, and inner membrane in green. Scale bar = 50 nm. (C) Tomographic slices of isolated wild-type and *ompB*^{STOP}::tn *R. parkeri* bacteria, paired with segmentation models of the bacterial membranes and S-layer in the XY and YZ planes color coded as in (B). (D) A tomographic slice from cryo-FIB-milled wild-type *R. parkeri* paired with a segmentation model of the bacterial membranes and S-layer in the XY plane. Scale bar = 100 nm. (iii) Expanded view of the bacterial surface indicated in the white box with arrowheads color coded as in (B). Purple asterisks denote examples of the slanted S-layer architecture. Scale bar = 20 nm.

Description

The *Rickettsia* genus comprises numerous species of arthropod-associated obligate-intracellular Gram-negative alphaproteobacteria, some of which are human pathogens causing various forms of rickettsiosis (Blanton, 2019). *Rickettsia parkeri*, which is endemic to the Americas and causes an eschar-associated spotted fever rickettsiosis (Paddock et al., 2004; Paddock et al., 2008), has emerged as a model for studying rickettsial infections. These bacteria invade host cells, escape from a membrane-bound phagosome, and grow within the host cell cytosol. Early electron microscopy images of various *Rickettsia* species noted the presence of a paracrystalline surface layer (S-layer) enmeshing the bacteria (Palmer et al., 1974; Popov and Ignatovich, 1976; Silverman et al., 1978). S-layers, which are found on most archaea and some bacteria, are ordered lattices that are formed by one or more S-layer proteins (Assandri et al., 2023; Grill-Walcher and Schäffer, 2025; Isbilir et al., 2026). Functions of the S-layer include membrane stabilization, microbe-microbe adhesion, and protection from phage infection (Assandri et al., 2023; Grill-Walcher and Schäffer, 2025). A high-resolution structure of the S-layer was determined for the related alphaproteobacterium *Caulobacter crescentus* using a combination of X-ray crystallography of the purified S-layer protein RsaA and cryo-electron tomography (cryoET) of intact bacteria (Bharat et al., 2017). The RsaA protomers fold into Ca^{2+}-coordinating β-helices that oligomerize to form a hexameric lattice (Bharat et al., 2017) that attaches to the LPS O-antigen on the surface of the bacterium (Awram and Smit, 2001; von Kügelgen et al., 2020). These studies provide a framework to investigate the structure of other alphaproteobacterial S-layers by cryoET.

The *Rickettsia* spp. S-layer has been proposed to be composed primarily of the outer membrane protein OmpB (Ching et al., 1990; Ching et al., 1996), which comprises approximately 10% of the total protein mass (Dasch et al., 1981). OmpB was originally characterized as a surface antigen (Dasch et al., 1981) and was subsequently shown to participate in host cell invasion (Chan et al., 2009) as well as protection from ubiquitylation and subsequent autophagy by the host cell (Engström et al., 2019; Engström et al., 2021). OmpB is conserved in *Rickettsia* species (Lehman et al., 2024) and is a member of the type V secretion system or autotransporter protein family (Blanc et al., 2005), consisting of an N-terminal passenger domain and C-terminal autotransporter domain. After translocation to the cell surface, OmpB is cleaved (Carl et al., 1990), leaving a 120 kDa fragment that is postulated to multimerize on the bacterial surface (Ching et al., 1990). Using AlphaFold 3 (Abramson et al., 2024), the structure of the passenger domain *R. parkeri* OmpB protein is predicted to fold into a series of β-sheets that emanate from the membrane-anchored autotransporter domain (Figure 1A), similar to the secondary structures in the *C. crescentus* RsaA protein (Bharat et al., 2017). However, whether OmpB is critical for the formation of the S-layer on the rickettsial surface has not been determined.

We imaged the bacterial surface by cryoET, first in an infected mammalian cell line, as the organism is obligately intracellular and thus best examined in its native context. Human A549 lung epithelial cells grown on holey carbon grids were infected with *R. parkeri*, and at 24 h post infection (hpi), were permeabilized for 30 s in the presence of both 0.5% Triton X-100 to facilitate cryoET of unmilled infected cells by removing cytoplasmic host cell material to reduce background noise, and 0.25% glutaraldehyde to gently fix and preserve protein structures (Urban et al., 2010; Mueller et al., 2014; Fäßler et al., 2020). Samples were then further fixed with 2% glutaraldehyde for at least 15 min and subsequently plunge frozen. CryoET imaging was carried out, targeting tilt series collection to thin regions of infected cells near the cell periphery. In tomograms containing bacteria, the inner and outer bacterial membranes were clearly visible, along with the S-layer surrounding the outer membrane (67 tomograms, 4 grids) (Figure 1B). To test whether OmpB is required to form the outer S-layer, we infected cells with the *R. parkeri ompB*^{STOP}::tn mutant, carrying both a nonsense mutation and transposon insertion in the *ompB* gene that minimally impact internalization of bacteria into hosts cells (Engström et al., 2019; Engström et al., 2021), and processed for imaging as described above. In tomograms of *R. parkeri ompB*^{STOP}::tn mutant bacteria, the inner and outer bacterial membranes were visible, but the outermost electron-dense S-layer was absent (16 tomograms, 1 grid) (Figure 1B). This indicates that OmpB is essential for S-layer formation and provides further evidence that OmpB is a major structural component of this layer.

To verify that permeabilization and fixation did not alter the presence of the S-layer, we purified bacteria from host cells, spotted them onto holey carbon grids, proceeded directly to plunge freezing without permeabilization or fixation, and then imaged using cryoET (Figure 1C). In these unfixed samples, the bacterial inner membrane appeared to be straighter, perhaps because permeabilization and fixation affected membrane structure. Moreover, the periplasmic space (distance between the inner and outer bacterial membranes) appeared to be larger and more variable in size, perhaps because

isolation of bacteria from the host cell environment caused a stress response. Nevertheless, in tomograms of isolated bacteria, the S-layer was again clearly visible on the surface of wild-type *R. parkeri* (34 tomograms, 1 grid), but absent in the *ompB*^{STOP}::tn mutant (47 tomograms, 1 grid) (Figure 1C).

To obtain higher-resolution tomograms of the bacterial surface, purified bacteria were further thinned through cryo-focused ion beam (cryo-FIB) milling (Khanna and Villa, 2022) after being spotted and plunge frozen on holey carbon grids (without permeabilization or fixation). Briefly, a gallium ion beam was used to mill away material from the top and bottom of the frozen bacterial lawn sample to a final thickness of about 200 nm. Following FIB-milling and cryoET imaging, the S-layer was better resolved, exhibiting a repetitive slanted lattice-like architecture (Figure 1D). We analyzed all tomograms comprising the cryo-FIB-milled dataset (22 tomograms, 2 grids) and found the external edge of the S-layer density is located an average of 14 ± 2 nm (SD) from the *R. parkeri* outer membrane, in the range of what was found for the S-layer or microcapsular layer in various negatively stained *Rickettsia* spp. samples (7-16 nm) (Palmer et al., 1974; Silverman et al., 1978) and slightly closer to the outer membrane than for *C. crescentus* (18-23 nm) (Bharat et al., 2017).

This study demonstrates the power of using cryoET to observe the *R. parkeri* surface. We confirmed the presence of an S-layer and demonstrated that the S-layer requires OmpB. Higher-resolution analysis of the OmpB structure and its association with other surface proteins and LPS will require the acquisition and subtomogram averaging of higher magnification tomograms of the bacterial surface. In addition to OmpB, the *Rickettsia* S-layer is proposed to contain OmpA (Ching et al., 1990; Ching et al., 1996), a larger and less abundant protein (OmpA:OmpB molar ratio is 1:9) (Policastro and Hackstadt, 1994). Similar to OmpB, OmpA is predicted to fold into a series of β-sheets, and the loss of OmpB may disrupt OmpA within the S-layer, compromising the lattice-like structure. Further structural analysis will be informative for determining how OmpB may interact with OmpA within the S-layer, as well as how OmpB shields OmpA and other surface proteins from ubiquitylation (Engström et al., 2019; Engström et al., 2021). This type of analysis will also be informative for understanding how the structure of the rickettsial S-layer compares with that of other microbes.

Methods

Mammalian cell culture

Vero (ATCC Cat# CCL-81, RRID:CVCL_0059) and A549 (ATCC Cat# CRM-CCL-185, RRID:CVCL_0023) cells were sourced from the University of California, Berkeley, Cell Culture Facility. Vero cells were grown in DMEM containing 4.5 g/L D-glucose, 4 mM L-glutamine (Gibco, 11965118), and 2% fetal bovine serum (Gemini Bio-products, 100-500). A549 cells were grown at 37 ˚C and 5% CO_2 in DMEM containing 4.5 g/L D-glucose, 4 mM L-glutamine (Gibco, 11965118), and 10% fetal bovine serum (ATLAS Biologics, FP-0500-A).

Rickettsia strain construction and propagation

R. parkeri strain Portsmouth was obtained from Chris Paddock at the Centers for Disease Control and Prevention. Fluorescent *R. parkeri* harboring pRAM18dR-GFPAa (Figueroa-Cuilan et al., 2023) were generated as described previously (Bacher et al., 2026). Briefly, a T75 flask of Vero cells infected with *R. parkeri* was harvested, resuspended in K36 buffer (50 mM KH_2PO_4, 50 mM K_2HPO_4, pH 7.0, 100 mM KCl, 15 mM NaCl), and broken open with 1 mm beads by two 30 s rounds of vortexing. Cell debris was pelleted at 10,000 rpm for 2 min at 4 ˚C, and the supernatant was washed 3× with 250 mM sucrose. Washed bacteria were resuspended in 100 µL brain heart infusion (BHI) media (BD Difco, DF0418-17-7) and incubated on ice for 20 min with 10 µg of the pRAM18dR-GFPAa plasmid. Bacteria were electroporated in a 0.2 cm cuvette (Bio-Rad, 165-2086) at 2.5 kV, 200 Ω, 25 µF, resuspended in 1.2 mL BHI media, and added to a new T75 flask of Vero cells. The next day, 500 ng/mL rifampicin (Sigma, R3501; resuspended to 1 mg/mL in methanol and filter sterilized) was added to the infected cells. Fluorescent *Rickettsia* were harvested from infected Vero cells by adding cold sterile water for 2 min to break bacteria out of the cells. Freed bacteria were pelleted, resuspended in BHI media, and frozen at -80 ˚C.

R. parkeri GFPAa (wild-type) and *R. parkeri ompB*^{STOP}::tn (Engström et al., 2019) bacteria were propagated and stored as a 30% preparation stock as described previously (Bacher et al., 2026). Briefly, *Rickettsia* bacteria were allowed to infect five confluent T175 flasks of Vero cells for 4-7 d at 33 ˚C. Infected cells were harvested, pelleted, and resuspended in 10 mL of K36 buffer. Bacteria were released from Vero cells by Dounce homogenization and isolated by centrifugation in a solution of 30% RenoCal-76 (Bracco Diagnostics, 04H208) in K36 buffer using a SW-32 Ti rotor (Beckman/Coulter) at 18,500 rpm for 30 min at 4 ˚C. The bacterial pellet was resuspended in 2 mL BHI media and aliquoted before freezing at -80 ˚C.

Preparation of EM grids with host cells infected with *R. parkeri*

Holey carbon grids (Quantifoil R2/1, 200 mesh, gold, SPI, 4320G-FA) were cleaned by treating with acetone for 20 min, blotted with Whatman No. 1 filter paper, and then treated with 70% ethanol for 20 min. For *ompB*^{STOP}::tn samples, grids were placed into 6-well plates with A549 cell culture media and incubated at 37 ˚C overnight. For wild-type samples, grids were placed into the wells of a 6-well plate with sterile water and then incubated in 0.1% poly-L-lysine (Sigma, P-

8920) for 15 min, and washed 2× with 1× PBS (Gibco, 10010-023) before A549 cell culture media was added for 1-24 h. Incorporation of a poly-L-lysine coating during grid preparation increased A549 cell adhesion and the total number of infected cells per grid. Once grids were primed in media, fresh A549 media was added to the wells with grids, A549 cells were dripped onto the grids, and seeded grids were incubated overnight at 37 ˚C in 5% CO_2. The next day, *R. parkeri* GFPAa or *R. parkeri ompB*^{STOP}::tn (MOI of 1-10) in cell culture media were added and grids were centrifuged at 300× g for 5 min. Infected cells were incubated for 24 h at 33 ˚C in 5% CO_2 and then fixed as described below and previously (Urban et al., 2010; Mueller et al., 2014; Fäßler et al., 2020).

For fixation, grids were transferred to a drop of 0.5% Triton X-100 (Sigma, T9284), 0.25% glutaraldehyde (EMS, 16120), and cytoskeleton buffer (10 mM MES, pH 6.8, 150 mM NaCl, 5 mM EGTA, 5 mM glucose, 5 mM $MgCl_2$) on parafilm for 30 s to permeabilize host cells. Grids were then moved to a drop of liquid containing 1 µg/mL unlabeled phalloidin (Sigma, P2141) or Alexa 568 phalloidin (Molecular Probes, A12380), 2% glutaraldehyde (EMS, 16120), and cytoskeleton buffer for at least 15 min for further fixation. Phalloidin was included to visualize bacterial actin tail structures, which is outside the scope of this study.

Post fixation, 7 µL of 10 nm gold beads (EMS, 25487, 6× concentrated) were pipetted onto the grids, the grids were blotted with Whatman No. 1 paper, and then another 3 µL of gold beads was added. Gold beads were used as fiducials for tomogram reconstruction. The grids were plunge-frozen in liquid ethane using an EM GP2 plunge freezer (Leica) after a 4-7 s blot. Grids were stored in liquid nitrogen until further use.

Preparation of EM grids with a bacterial lawn

Grids were prepared using a protocol adapted from Khanna and Welch, 2024. Holey carbon grids (Quantifoil R2/1, 200 mesh, copper, EMS, Q2100CR1; Quantifoil R2/1, 200 mesh, gold, SPI, 4320G-FA; or Quantifoil R1/2, 200 mesh, gold, EMS, Q2100AR-12,) were glow discharged for 10 s at 15 mA using a Pelco easiGlow system (RRID:SCR_020396). A total of 7 µL of *R. parkeri* GFPAa or *R. parkeri ompB*^{STOP}::tn bacteria (3.5-5×10^7 bacteria) from a frozen 30% preparation stock were spotted onto a grid as follows. Half (3.5 µL) of the bacterial volume was pipetted, the grid was blotted with Whatman No. 1 filter paper, and then the other half of the bacterial volume (3.5 µL) was added. The grids were plunge-frozen in liquid ethane using an EM GP2 plunge freezer (Leica) after a 4-7 s blot. Grids were stored in liquid nitrogen until further use.

For cryo-FIB-milling, grids were transferred to the Stanford-SLAC CryoET Specimen Preparation Center (SCSC) and loaded into an Aquilos 2 Cryo-FIB microscope (ThermoFisher Scientific, RRID:SCR_019880) for milling with a 30 kV focused ion beam. Grids were sputter coated with metallic platinum, coated with organometallic platinum using a gas injection system for 1 min, and then sputter-coated again with metallic platinum. AutoTEM 5 software (ThermoFisher) was used to determine the milling angle for all lamella sites. For some samples, the AutoTEM 5 software (ThermoFisher) was used to completely mill lamellae to a thickness of 200 nm. Incompletely milled lamellae were manually milled with 500 pA (rough milling) that was gradually reduced to 30 pA (polishing) to obtain 200 nm thick lamellae. Stress relief cuts were included to limit lamellae breakage.

Tilt series collection and processing

For the *ompB*^{STOP}::tn sample in Figure 1B, tilt series were collected at UC Berkeley CalCryo@QB3 facility using a Titan Krios (FEI) operated at 300 kV and equipped with a K2 direct electron detection device (Gatan) and quantum energy filter (Gatan). Images were collected at a 3.36 Å pixel size and with a target defocus of -6 µm. Automated tilt series acquisition was performed using Serial EM v4.0.12 (Mastronarde, 2005) using a bidirectional tilt scheme with an increment of 2˚ and a total electron dose of 120 $e^-/Å^2$.

For Figures 1B wild-type, 1C, and 1D, tilt series were collected at the UW Madison Cryo-EM Research Center Midwest Center for Cryo-Electron Tomography (MCCET). Tilt series were acquired on a Titan Krios (ThermoFisher) at 300 kV equipped with a K3 electron detection device (Gatan) and quantum energy filter (Gatan) using Serial EM v4.1.0 (Mastronarde, 2005).

For Figure 1B, wild-type, automated tilt series were acquired at a pixel size of 3.7 Å and target defocus of -6 µm using a dose-symmetric tilt scheme with increments of 3˚ and a total electron dose of 120 $e^-/Å^2$. For Figure 1C, wild-type, automated tilt series were acquired at a pixel size of 3 Å and target defocus of -4 to -6 µm using a dose-symmetric tilt scheme with increments of 3˚ and a total electron dose of 120 $e^-/Å^2$. For Figure 1C, *ompB*^{STOP}::tn, automated tilt series were acquired at a pixel size of 1.9 Å and target defocus of -6 µm using a dose-symmetric tilt scheme with increments of 3˚ and a total electron dose of 100 $e^-/Å^2$. For Figure 1D, automated tilt series were acquired at a pixel size of 2.4 Å and target defocus of -3 to -5 µm using a dose-symmetric tilt scheme with increments of 3˚ and a total electron dose of 100 $e^-/Å^2$.

For initial screening of tomograms, tilt series were motion corrected with MotionCor2 1.6.4 (Zheng et al., 2017) and then aligned and reconstructed using AreTomo2 v1.1.2 (Zheng et al., 2022). For final reconstruction of tomograms with fixed

infected cells, tilt series were aligned in IMOD v5.1 (Kremer et al., 1996) (RRID:SCR_003297) using the 10 nm gold beads as fiducials for alignment and weighted back-projection algorithm with a simultaneous iterative reconstruction technique (SIRT)-like filter. Tomograms were binned by a factor of 3 and then processed with the nonlinear anisotropic diffusion (NAD) filter. For final reconstruction and visualization of tomograms without gold fiducials, tilt series were motion-corrected using Relion 5.0 and aligned using AreTomo2 default parameters through the wrapper within Relion 5.0 (Burt et al., 2024) (RRID:SCR_016274). Contrast transfer function (CTF) estimation was also performed with AreTomo2 during tilt series alignment. Tomogram reconstruction was performed in Relion 5.0 after removal of dark images and tomograms were binned to a pixel size of 10 Å.

Tomogram segmentation and S-layer quantification

For Figures 1C and 1D, manual segmentation of 27-75 slices of representative wild-type and *ompB*^{STOP}::tn tomograms was performed in Dragonfly 3D (v2025.1; Comet Technologies Inc.). The S-layer thickness (edge of outer membrane density to outer edge of S-layer density) of wild-type FIB-milled bacteria was measured at two locations per tomogram using the contour modeling function in IMOD v4.11.25 (Kremer et al., 1996).

Data availability

Tomograms have been deposited to the Biohub CryoET Data Portal database under deposition code: CZCDP-10353.

Reagents

Strain	**Genotype**	**Reference**
R. parkeri GFPAa (wild-type)	*R. parkeri* strain Portsmouth harboring the pRAM18dR-GFPAa shuttle vector	This study
R. parkeri *ompB*^{STOP}::tn	*ompB* null *R. parkeri* strain Portsmouth harboring both a nonsense mutation and a transposon insertion in the *ompB* gene	Engström et al., 2019
Plasmid	**Genotype**	**Description**
GFPAa	pRAM18dR-GFPAa	GFPuv in pRAM19dRGA is replaced with AausFP1. From Figueroa-Cuilan et al., 2023.

Acknowledgements: We thank Kanika Khanna, who advised on bacterial lawn sample preparation and commented on the manuscript. We thank Lydia-Marie Joubert, Yang Xu, and Pingting Liu at the Stanford-SLAC CryoET Specimen Preparation Center (SCSC). We also thank Bryan Sibert, Yumeng Liu, and Anna Ratliff at the Midwest Center for CryoET (MCCET) for assistance with cryoET data acquisition. We thank Hang Cheng for guidance with tomogram processing and segmentation. We thank Erin Goley for providing the pRAM18dR-GFPAa plasmid for using in making fluorescent *R. parkeri*.

References

Abramson J, Adler J, Dunger J, Evans R, Green T, Pritzel A, et al., Jumper JM. 2024. Accurate structure prediction of biomolecular interactions with AlphaFold 3. Nature 630(8016): 493-500. PubMed ID: 38718835

Assandri MH, Malamud M, Trejo FM, Serradell MLA. 2023. S-layer proteins as immune players: Tales from pathogenic and non-pathogenic bacteria. Curr Res Microb Sci 4: 100187. PubMed ID: 37064268

Awram P, Smit J. 2001. Identification of lipopolysaccharide O antigen synthesis genes required for attachment of the S-layer of *Caulobacter crescentus*. Microbiology (Reading) 147(Pt 6): 1451-1460. PubMed ID: 11390676

Bacher MC, Choe JE, Jiang J, Idrovo JM, Del Mundo JT, Hammel M, Welch MD. 2026. Divergent *Rickettsia* species exhibit distinct mechanisms of actin-based motility. J Cell Biol 225(7): 10.1083/jcb.202508117. PubMed ID: 42048062

Bharat TAM, Kureisaite-Ciziene D, Hardy GG, Yu EW, Devant JM, Hagen WJH, et al., Löwe J. 2017. Structure of the hexagonal surface layer on *Caulobacter crescentus* cells. Nat Microbiol 2: 17059. PubMed ID: 28418382

Blanc G, Ngwamidiba M, Ogata H, Fournier PE, Claverie JM, Raoult D. 2005. Molecular evolution of *Rickettsia* surface antigens: evidence of positive selection. Mol Biol Evol 22(10): 2073-83. PubMed ID: 15972845

Blanton LS. 2019. The rickettsioses: A practical update. Infect Dis Clin North Am 33(1): 213-229. PubMed ID: 30712763

Burt A, Toader B, Warshamanage R, von Kügelgen A, Pyle E, Zivanov J, et al., Scheres SHW. 2024. An image processing pipeline for electron cryo-tomography in RELION-5. FEBS Open Bio 14(11): 1788-1804. PubMed ID: 39147729

Carl M, Dobson ME, Ching WM, Dasch GA. 1990. Characterization of the gene encoding the protective paracrystalline-surface-layer protein of *Rickettsia prowazekii*: presence of a truncated identical homolog in *Rickettsia typhi*. Proc Natl Acad Sci U S A 87(21): 8237-41. PubMed ID: 2122457

Chan YG, Cardwell MM, Hermanas TM, Uchiyama T, Martinez JJ. 2009. Rickettsial outer-membrane protein B (rOmpB) mediates bacterial invasion through Ku70 in an actin, c-Cbl, clathrin and caveolin 2-dependent manner. Cell Microbiol 11(4): 629-44. PubMed ID: 19134120

Ching WM, Dasch GA, Carl M, Dobson ME. 1990. Structural analyses of the 120-kDa serotype protein antigens of typhus group rickettsiae. Comparison with other S-layer proteins. Ann N Y Acad Sci 590: 334-51. PubMed ID: 2116106

Ching WM, Wang H, Jan B, Dasch GA. 1996. Identification and characterization of epitopes on the 120-kilodalton surface protein antigen of *Rickettsia prowazekii* with synthetic peptides. Infect Immun 64(4): 1413-9. PubMed ID: 8606109

Dasch GA, Samms JR, Williams JC. 1981. Partial purification and characterization of the major species-specific protein antigens of *Rickettsia typhi* and *Rickettsia prowazekii* identified by rocket immunoelectrophoresis. Infect Immun 31(1): 276-88. PubMed ID: 6783537

Engström P, Burke TP, Mitchell G, Ingabire N, Mark KG, Golovkine G, et al., Welch MD. 2019. Evasion of autophagy mediated by *Rickettsia* surface protein OmpB is critical for virulence. Nat Microbiol 4(12): 2538-2551. PubMed ID: 31611642

Engström P, Burke TP, Tran CJ, Iavarone AT, Welch MD. 2021. Lysine methylation shields an intracellular pathogen from ubiquitylation and autophagy. Sci Adv 7(26): 10.1126/sciadv.abg2517. PubMed ID: 34172444

Fäßler F, Dimchev G, Hodirnau VV, Wan W, Schur FKM. 2020. Cryo-electron tomography structure of Arp2/3 complex in cells reveals new insights into the branch junction. Nat Commun 11(1): 6437. PubMed ID: 33353942

Figueroa-Cuilan WM, Irazoki O, Feeley M, Smith E, Nguyen T, Cava F, Goley ED. 2023. Quantitative analysis of morphogenesis and growth dynamics in an obligate intracellular bacterium. Mol Biol Cell 34(7): ar69. PubMed ID: 37017481

Grill-Walcher S, Schäffer C. 2025. A new age in structural S-layer biology: Experimental and in silico milestones. J Biol Chem 301(6): 110205. PubMed ID: 40345586

Isbilir B, von Kügelgen A, Alva V, Bharat TAM. 2026. Assembly, architecture and functional roles of microbial surface layers. Nat Rev Microbiol 24(5): 344-358. PubMed ID: 41233633

Khanna K, Villa E. 2022. Revealing bacterial cell biology using cryo-electron tomography. Curr Opin Struct Biol 75: 102419. PubMed ID: 35820259

Khanna K, Welch MD. 2024. Cryo-electron tomography of stationary phase *Burkholderia thailandensis*. MicroPubl Biol 2024: 10.17912/micropub.biology.001178. PubMed ID: 38725941

Kremer JR, Mastronarde DN, McIntosh JR. 1996. Computer visualization of three-dimensional image data using IMOD. J Struct Biol 116(1): 71-6. PubMed ID: 8742726

Lehman SS, Verhoeve VI, Driscoll TP, Beckmann JF, Gillespie JJ. 2024. Metagenome diversity illuminates the origins of pathogen effectors. mBio 15(5): e0075923. PubMed ID: 38564675

Mastronarde DN. 2005. Automated electron microscope tomography using robust prediction of specimen movements. J Struct Biol 152(1): 36-51. PubMed ID: 16182563

Mueller J, Pfanzelter J, Winkler C, Narita A, Le Clainche C, Nemethova M, et al., Small JV. 2014. Electron tomography and simulation of baculovirus actin comet tails support a tethered filament model of pathogen propulsion. PLoS Biol 12(1): e1001765. PubMed ID: 24453943

Paddock CD, Finley RW, Wright CS, Robinson HN, Schrodt BJ, Lane CC, et al., Eremeeva ME. 2008. *Rickettsia parkeri* rickettsiosis and its clinical distinction from Rocky Mountain spotted fever. Clin Infect Dis 47(9): 1188-96. PubMed ID: 18808353

Paddock CD, Sumner JW, Comer JA, Zaki SR, Goldsmith CS, Goddard J, et al., Ohl CA. 2004. *Rickettsia parkeri*: a newly recognized cause of spotted fever rickettsiosis in the United States. Clin Infect Dis 38(6): 805-11. PubMed ID: 14999622

Palmer EL, Martin ML, Mallavia L. 1974. Ultrastucture of the surface of *Rickettsia prowazeki* and *Rickettsia akari*. Appl Microbiol 28(4): 713-6. PubMed ID: 4138139

Policastro PF, Hackstadt T. 1994. Differential activity of *Rickettsia rickettsii* opmA and ompB promoter regions in a heterologous reporter gene system. Microbiology (Reading) 140 (Pt 11): 2941-9. PubMed ID: 7812435

Popov VL, Ignatovich VF. 1976. Electron microscopy of surface structures of *Rickettsia prowazeki* stained with ruthenium red. Acta Virol 20(5): 424-8. PubMed ID: 63238

Silverman DJ, Wisseman CL Jr, Waddell AD, Jones M. 1978. External layers of *Rickettsia prowazekii* and *Rickettsia rickettsii*: occurrence of a slime layer. Infect Immun 22(1): 233-46. PubMed ID: 83297

Urban E, Jacob S, Nemethova M, Resch GP, Small JV. 2010. Electron tomography reveals unbranched networks of actin filaments in lamellipodia. Nat Cell Biol 12(5): 429-35. PubMed ID: 20418872

von Kügelgen A, Tang H, Hardy GG, Kureisaite-Ciziene D, Brun YV, Stansfeld PJ, Robinson CV, Bharat TAM. 2020. In situ structure of an intact lipopolysaccharide-bound bacterial surface layer. Cell 180(2): 348-358.e15. PubMed ID: 31883796

Zheng S, Wolff G, Greenan G, Chen Z, Faas FGA, Bárcena M, et al., Agard DA. 2022. AreTomo: An integrated software package for automated marker-free, motion-corrected cryo-electron tomographic alignment and reconstruction. J Struct Biol X 6: 100068. PubMed ID: 35601683

Zheng SQ, Palovcak E, Armache JP, Verba KA, Cheng Y, Agard DA. 2017. MotionCor2: anisotropic correction of beam-induced motion for improved cryo-electron microscopy. Nat Methods 14(4): 331-332. PubMed ID: 28250466

Funding: This work was funded by grant R01 AI109044 from the National Institute of Allergy and Infectious Diseases (NIAID), National Institutes of Health (NIH), Department of Health and Human Services (DHHS), awarded to M.D.W. This project was funded in part with federal funds from the NIAID, NIH, DHHS, under Contract 75N93022C00035, awarded to D.B. Tomogram reconstruction was supported by the Structural Biology Lab at UT Southwestern Medical Center, which is partially supported by grant RP220582 from the Cancer Prevention & Research Institute of Texas (CPRIT). Some of this work was performed at Stanford-SLAC CryoET Specimen Preparation Center (SCSC) and the Midwest Center for Cryo-Electron Tomography (MCCET) and the Cryo-EM Research Center, located in the Department of Biochemistry at the University of Wisconsin-Madison, supported by the NIH Common Fund's Transformative High Resolution Cryo-electron Microscopy Program (U24 GM-139166 and U24 GM-139168). D.S. was supported by a Human Frontier Science Program long-term fellowship LT000234/2018-L.
Supported by National Institute of Allergy and Infectious Diseases (United States) R01 AI109044 to M.D.W..
Supported by National Institute of Allergy and Infectious Diseases (United States) Contract 75N93022C00035 to D.B..
Supported by Cancer Prevention and Research Institute of Texas (United States) RP220582 to Structural Biology Lab at UT Southwestern Medical Center.
Supported by NIH Common Fund (United States) U24 GM-139166 to Stanford-SLAC CryoET Specimen Preparation Center (SCSC).
Supported by NIH Common Fund (United States) U24 GM-139168 to Midwest Center for Cryo-Electron Tomography (MCCET).

Conflicts of Interest: D.B. is a co-founder of Ligo Analytics, a company that develops software for cryogenic electron microscopy.

Author Contributions: Meghan C. Bacher: conceptualization, data curation, formal analysis, investigation, validation, visualization, writing - original draft. Daniel Serwas: data curation, investigation, methodology, visualization, writing - review editing. Yan Han: formal analysis, methodology, validation, writing - review editing. Dominika Borek: funding acquisition, methodology, supervision, writing - review editing. Matthew D. Welch: conceptualization, funding acquisition, project administration, supervision, writing - review editing.

Reviewed By: Anonymous

History: Received May 27, 2026 **Revision Received** June 11, 2026 **Accepted** June 12, 2026 **Published Online** June 16, 2026 **Indexed** June 30, 2026

Citation: Bacher MC, Serwas D, Han Y, Borek D, Welch MD. 2026. Cryo-electron tomography reveals OmpB is required for the *Rickettsia parkeri* S-layer. microPublication Biology. 10.17912/micropub.biology.002219